Macromolecular Bioscience
www.mbs-journal.de

Usnic-Acid-Functionalized Silk Fibroin Composite Scaffolds for Cutaneous Wounds Healing

*Xiaoying Zha, Xingliang Xiong, Cheng Chen, Yang Li, Lingqin Zhang, Haojiang Xie, and Qifeng Jiang**

Despite the progress in chronic wound treatment, antibacterial cutaneous scaffold with high efficiency in wound healing is still the hot spot in the field. In present study, a functionalized silk fibroin (SF) cutaneous scaffold incorporated with natural medicine usnic acid (UA) is investigated, in which UA is used as an antibacterial and wound-healing reagent. Via electrospinning, UA–SF mixture is fabricated into UA–SF composite scaffold (USCS), which is composed of uniform nanofibers with average diameters of around 360 ± 10 nm. The interwoven nanofibers form mesh structure providing sufficient moisture permeability for scaffold. With methanol treatment, USCS presents improved mechanical properties and stability to protease XIV. In the presence of USCS, the growth rate of both Gram-positive and Gram-negative bacteria, including *Staphylococcus aureus, Streptococci pyogenes, Escherichia coli*, and *Pseudomonas aeruginosa*, is significantly inhibited in plate culture and suspension assays. In a cutaneous excisional mouse wound model, USCS presents a significant increase of wound closure rate, compared with pure SF scaffold and commercial dressing, Tegaderm Hydrocolloid 3M. The histological assessments further prove that USCS can enhance re-epithelialization, vascularization, and collagen deposition in wound site to promote the wound-healing process, which indicates the potential application of USCS in chronic wound treatment.

1. Introduction

As the largest organ in human body, skin is an important part for maintaining the stability of internal environment and normal physiological functions of body. Chronic cutaneous wounds often destroy the integrity of skin, resulting in severe damage to human body, like bacterial infection, inflammation, and tissue necrosis.[1] For efficient wound treatment, wound dressing is frequently used to restore the normal function of skin and to enhance wound healing. Theoretically, an ideal wound dressing should possess the advantages of antibacterial activity, biocompatibility, gas permeability, and tunable mechanical properties.[1]

As a natural protein extracted from the *Bombyx mori* silk worm cocoon,[2] silk fibroin (SF) has been considered as an exceptional polymer matrix for biomedical application due to its controllable degradability,[3,4] excellent biocompatibility,[5] and tunable mechanical properties.[6–8] SF can be easily engineered into different structures including tubes,[9] hydrogels,[10,11] freeze-dried sponges,[5,12,13] electrospun mats,[14–16] films,[17–19] and microspheres.[20,21] Previous study has demonstrated that SF-based wound dressings could accelerate wound closure with less inflammation than commercial wound-healing product, DuoActive dressing.[22] More importantly, SF could be generated in aqueous state under relative mild conditions which make it an attractive material for sensitive biologics loading.[16] Previous study has shown that antibiotic could be efficiently loaded into SF to further functionalize the material with antibacterial and wound-healing activities.[23] However, more or less, the SF materials mixed with certain antibiotics always confront the issue of allergy or drug resistance, which is intensively considered in clinical application.[24]

As a metabolite of lichen, the natural medicine usnic acid (UA) is a secondary lichen metabolite extensively studied for the broad variety of biological features,[25] and it has great potential in pharmacology and clinic due to its unique characteristics such as antibacterial, anti-inflammatory, antiviral, and biocompatibility.[25,26] Previous studies showed that UA reduced the bacterial infection in a mouse model without detectable toxicity and drug resistance, which might give UA a bright future in infection treatment.[27–29] Besides, NaUA, synthesized by a chemical reaction of UA and sodium salt, could significantly facilitate wound closure in a full-thickness cutaneous excisional mouse wound model.[30] Additionally, bactericidal activity of UA-loaded electrospun fibers of Eudragit L-100 and polyvinylpyrrolidone was examined against *Staphylococcus aureus*.[31] Moreover, previous study has successfully loaded UA into a polymer matrix, NaCMC to prepare a bioadhesive film by gels'

X. Zha, Prof. X. Xiong, Prof. C. Chen, L. Zhang, H. Xie, Prof. Q. Jiang
Medical Information College
Chongqing Medical University
Chongqing 400016, China
E-mail: jiangqf@cqmu.edu.cn
Y. Li
Department of Medical Equipment
Yubei District People's Hospital
Chongqing 401120, China
The ORCID identification number(s) for the author(s) of this article can be found under https://doi.org/10.1002/mabi.202000361.

DOI: 10.1002/mabi.202000361

casting, which presented significantly antibacterial properties, cytocompatibility, and promotion in wound healing.[32]

Although SF-based materials and UA-loading dressings are booming, there is little specific research focus on potential application in clinics based on combination of SF and UA. In the present study, we novelty proposed an antibacterial cutaneous scaffold, UA–SF composite scaffold (USCS), via electrospinning. First, mechanical properties and degradation stability of USCS were optimized with tunable fabrication parameters. Second, antibacterial activities of USCS were demonstrated by growth inhibition on Gram-positive and Gram-negative bacteria including *S. aureus, Streptococci pyogenes, Escherichia coli, and Pseudomonas aeruginosa*. Third, a cutaneous excisional mouse wound model was used to evaluate the wound-healing effect of USCS, and the possible mechanism of wound-healing promotion was also probed with the histological assessment of wound tissue. Compared with traditional wound dressings such as Tegaderm Hydrocolloid ^{3M}, USCS not only presented much better antibacterial activities and wound-healing effect, but also obtained much improved gas permeability and mechanical properties, which indicated that combination of UA and SF might provide a potential strategy for clinical treatment with chronic wound.

2. Results and Discussion

2.1. Characterization of Composite Scaffolds

The surface morphology and internal fiber network of scaffolds were explored by scanning electron microscopy (SEM) images. More detailed information about surface morphology of scaffolds, processing parameters during electrospinning, and average diameter of nanofibers is listed in Figure S1 and Table S1 (Supporting Information). Scaffolds from 18 wt% SF concentration were accompanied by droplets, and the diameter of nanofibers was not uniform (**Figure 1**a–c); however, the concentration of UA (0.5%) had no effect on the structure of scaffolds (Figure 1d). As shown in Figure 1e–g, scaffolds from 20 wt% SF concentration presented uniform fibrous structures with the average diameter of nanofibers being around 360 ± 10 nm. The nanofibers are interwoven with each other to form a mesh structure which was supposed to guarantee UA sufficient loading and continuous release. Similarly, UA concentration up to 0.5% had no significant influence on fibrous structure of scaffolds, in which the average diameter of nanofibers was around 365 ± 10 nm (Figure 1h). The SF concentration of 20 wt% was chosen for following studies.

Previous studies have shown that methanol treatment could control the mechanical properties of SF nonwoven fabrics by changing the β-sheet content.[8,14] In this work, methanol was used to induce β-sheet formation inside SF nanofibers to improve both mechanical and biological stability of the scaffold. The secondary structure at amide I region in scaffolds was investigated by Fourier transform infrared spectroscopy (FTIR) analysis. As shown in **Figure 2**a, in the FTIR spectra, an absorption peak at 1644 cm^{-1} was observed in untreated scaffolds attributed to the noncrystalline structure, such as α-helix (1600–1615 cm^{-1}, 1711–1720 cm^{-1}), random coil (1641–1646 cm^{-1}) and β-turn (1661–1685 cm^{-1}), which were consistent with previous studies.[15,33] In contrast, the intensity of β-sheet at 1631 cm^{-1} was significantly increased after methanol treatment, indicating an increase of the β-sheet content (Figure 2a,b). Furthermore, Fourier self-deconvolution to the original spectra was performed followed by curve fitting (Figure 2c,d).[7,15] Figure 2b shows the content of β-sheet increased after treatment (from 15.45% to 50.27%) while the content of noncrystalline structure decreased (α-helix: from 11.81% to 8.52%; random coil: from 34.21% to 3.14%). The increase of β-sheet content induced by methanol treatment provided an efficient way to tune the mechanical properties and stability of scaffolds.[4,7]

2.2. Performance of USCS

Tunable mechanical property is an important factor for cutaneous scaffold, which theoretically can be customized for

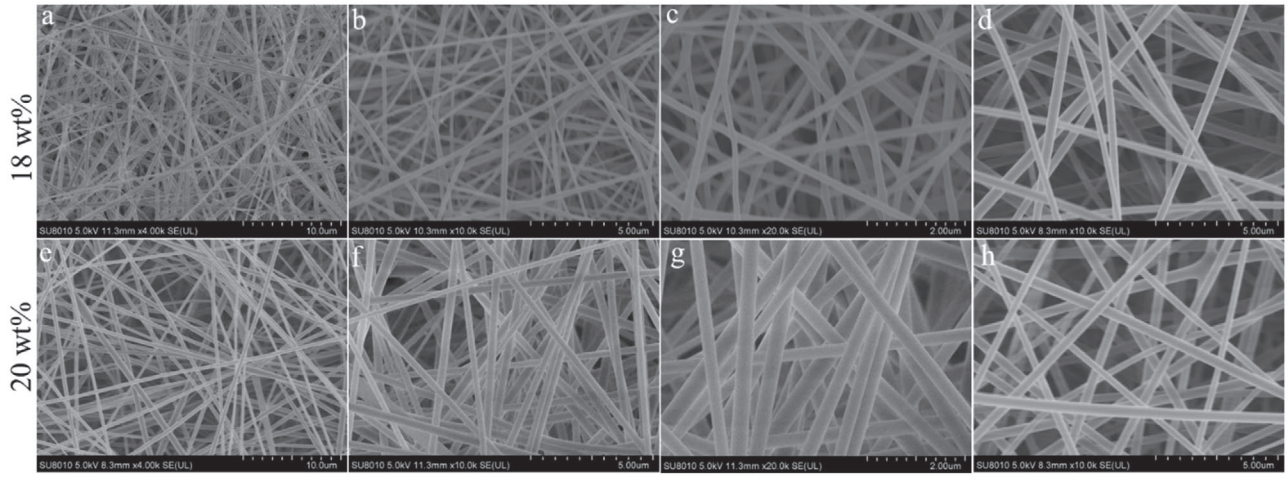

Figure 1. Characterization of USCS with SEM. a–c) Pure SF scaffolds with the concentration of 18 wt% under different magnifications of 4, 10, and 20 k, respectively. d) USCS loading of 0.5% UA under magnification of 10 k. e–g) Pure SF scaffolds with the concentration of 20 wt% under different magnifications of 4, 10, and 20 k, respectively. h) USCS loading of 0.5% UA under magnification of 10 k.

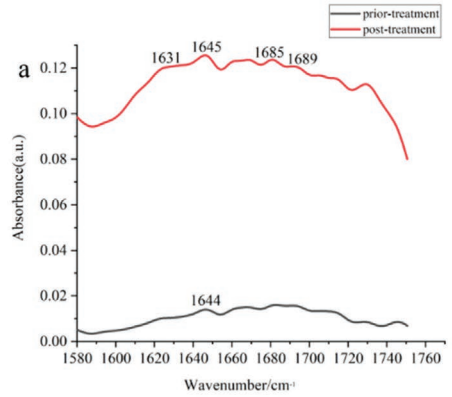

b

Wavenumber range (cm^{-1})	Assignment	Prio-treatment percentage(%)	Post-treatment percentage(%)
1600 - 1615	α helix	4.40	3.97
1616 - 1635	β-sheet	6.87	28.48
1641 - 1646	random coils	34.21	3.14
1661 - 1685	turn	38.53	38.07
1686 - 1710	β-sheet	8.58	21.79
1711 - 1720	α helix	7.41	4.55

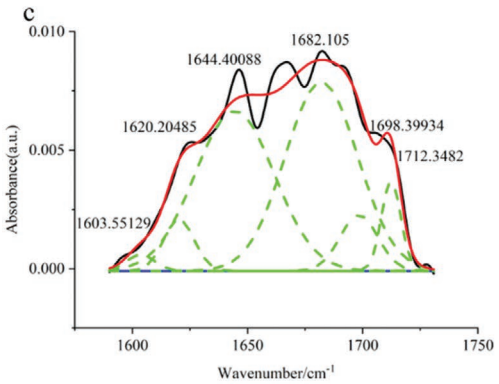

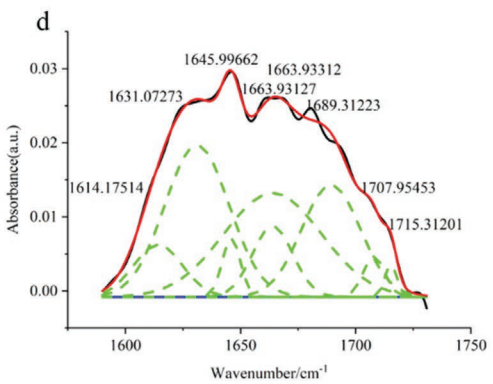

Figure 2. a) FTIR analysis of scaffolds prior and post treatment by methanol with original FTIR absorbance spectra of amide I region between 1750 and 1580 cm^{-1}, the fractions distribution of different SF conformations in amide I region. b) Content of different conformations in SF before and after methanol treatment. c) Curve fitting from Fourier self-deconvolution to the original spectra before methanol treatment (blue/black/red/green line indicates baseline/subtracted data (the original peak subtract the baseline)/fitting curve/hidden peak). d) Curve fitting from Fourier self-deconvolution to the original spectra after methanol treatment (blue/black/red/green line indicates baseline/subtracted data (the original peak subtract the baseline)/fitting curve/hidden peak).

different wound site.[1] In this study, stress–strain curves and ultimate tensile strength (UTS) were tested to determine the mechanical properties of USCS. As shown in **Figure 3**, before methanol treatment, the USCS from 18 wt% concentration was easy to fracture with elongation break point at only 0.92%; however, the flexibility of USCS was significantly improved when concentration reached 20 wt% (2.52%). Methanol treatment could slightly promote the flexibility of USCS with both 18 and 20 wt% concentration, increasing the elongation break point to 1.28% and 2.98%, respectively (Figure 3a), which might indicate SF concentration is the main factor for USCS flexibility rather than β-sheet content induced by methanol treatment. Furthermore, before methanol treatment, lower SF concentration (18 wt%) presented lower UTS which was 1.03 ± 0.18 MPa (Figure 3b), by increasing SF concentration to 20 wt%, the UTS could be up to 1.68 ± 0.41 MPa (Figure 3c). After methanol treatment, the UTS values of scaffolds from 18 wt% and 20 wt% SF were both significantly increased to 1.69 ± 0.45 and 2.61 ± 0.61 MPa, respectively. This change might be attributed to the increase of β-sheet formation in scaffolds induced by methanol, which caused contraction and higher packing density of the fiber mats, which are often thought to result in enhanced stiffness in dry mechanical tests.[4,8] Moreover, the content of UA (0.5%) had no significant influence on UTS of scaffolds with different SF concentrations. This might be because UA was simply mixed in the mesh structure of USCS, instead of high affinity binding, which provided convenient way for UA release.

The degradation rate is another feature should be considered for cutaneous scaffold, especially in the presence of enzyme. In present work, degradation of USCS to protease XIV at different time points was studied in vitro. As shown in Figure 3d,e, it only took 5 days for USCS with 18 wt% SF concentration to degrade to 5.8% of its original mass. However, increasing SF concentration would improve the resistance of USCS to protease XIV and USCS with 20 wt% SF concentration required 8 days to degrade to 11.36% of its original mass. Methanol treatment promoted the stability of USCS to protease XIV in both 18 wt% and 20 wt% SF concentration groups and the time prolonged to 9 and 14 days for each group to degrade to the similar remaining mass ratio. The decreased degradation rate of USCS after methanol treatment could be related to the promotion of the β-sheet formation induced by methanol, which leads USCS to maintain mechanical integrity and insoluble in water.[3–5] Therefore, the degradation of USCS could be easily manipulated with different concentrations of SF or methanol treatment.

Because accumulation of interstitial fluid at wound site may lead to inflammation and even ulceration of the wound, it is desirable for cutaneous scaffold to have enough permeability, which can be referred to water vapor transmission rate (WVTR) index.[34]

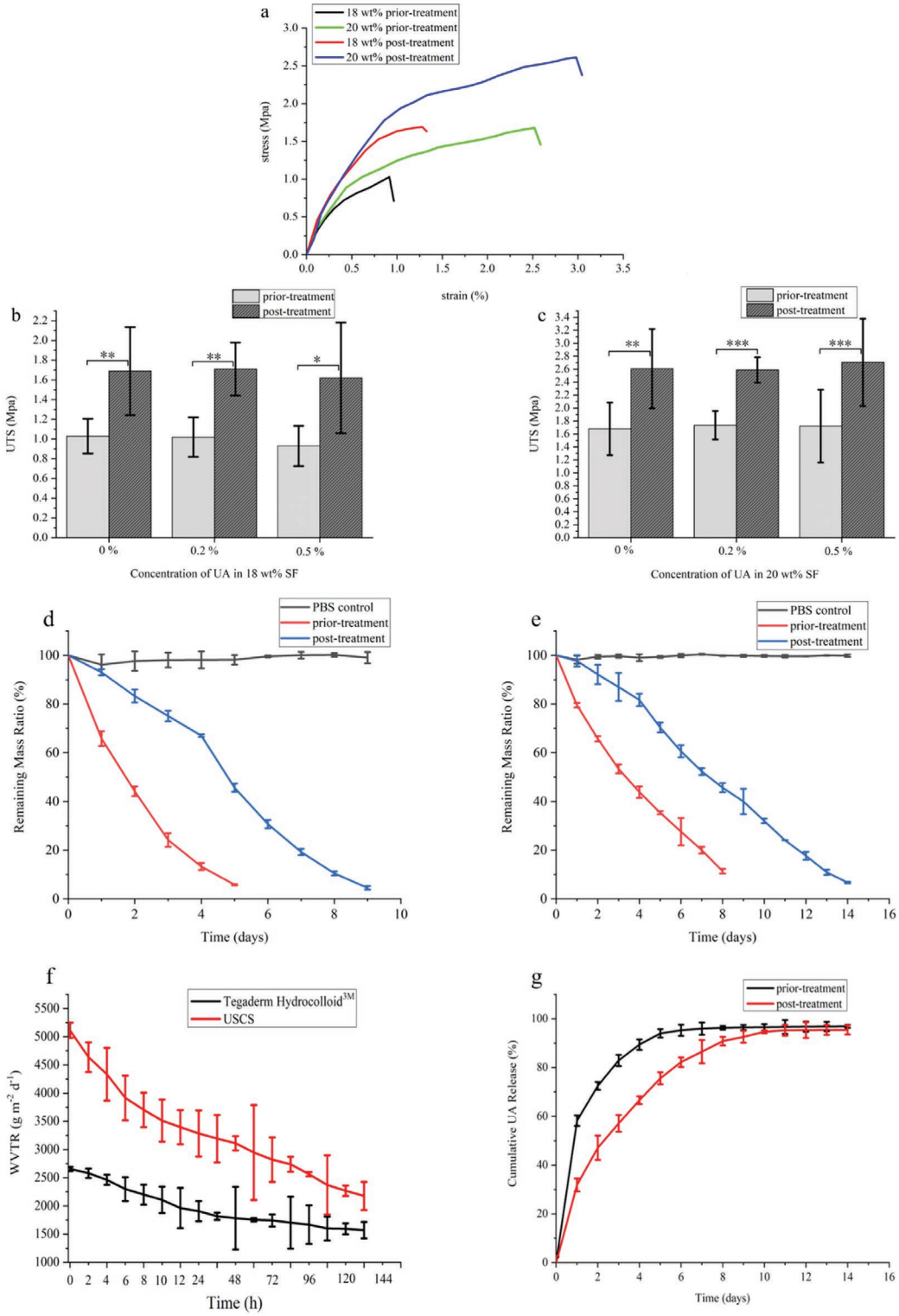

Figure 3. a) Stress–strain curves of USCS obtained in the tensile test. USCS from 20 wt% SF concentration (green curve) presented much enhanced flexibility compared with 18 wt% SF concentration (black curve). Methanol treatment slightly improved flexibility of USCS from both 18 wt% (red curve) and 20 wt% (blue curve) SF concentrations. b) The changes in UTS of scaffolds from 18 wt% SF before and after treatment by methanol. c) The changes in UTS of scaffolds from 20 wt% SF before and after treatment by methanol. d) Degradation rate of USCS from 18 wt% SF in protease XIV before (red line) and after (blue line) treatment by methanol. e) Degradation rate of USCS from 20 wt% SF in protease XIV before (red line) and after (blue line) treatment by methanol; black lines represent the weight changes of USCS treated with PBS. f) WVTR of USCS and Tegaderm Hydrocolloid 3M over time. g) UA sustained release from USCS before and after methanol treatment.

The WVTR for USCS was ≈5112.8 ± 134.9 g m^{-2} d^{-1} at the beginning, then decreased gradually to 2177.3 ± 249.5 g m^{-2} d^{-1} till 132 h, By comparison, the WVTR of commercial product, Tegaderm Hydrocolloid ^{3M} was only about 2656.8 ± 37.7 g m^{-2} d^{-1} at the beginning, then decreased gradually to 2177.3 ± 249.5 g m^{-2} d^{-1} till 132 h. It is worth noting that WVTR of USCS after 132 h was very similar to fresh Tegaderm Hydrocolloid ^{3M} (Figure 3f). Like most traditional bandages, Tegaderm Hydrocolloid ^{3M} has thick texture and most of the evaporated water was absorbed by themselves and cannot be sent out timely; this is the reason why traditional bandages "whiten" the wounds and even stinking.[35] These results showed that USCS exhibited excellent air permeability, which could probably accelerate wound healing.

In this work we found that changes in the secondary structure of USCS might control the release behavior of UA. As shown in Figure 3g, a burst release of UA was observed in USCS without methanol treatment, and UA up to 58.2% was released at the first day, and nearly completely released by the fourth day. In contrast, after methanol treatment, UA release was only about 31.9% at the first day, and the full release took up to 10 days even longer. This might because the β-sheets formation induced by methanol made USCS inner structure more stable and compact in the presence of water, resulting in slower and sustained UA release.[27]

2.3. Antibacterial Effects of USCS

To examine the antibacterial activity of USCS, we performed the inhibition zone test and suspension assays against Gram-negative bacteria (*E. coli* and *P. aeruginosa*) and Gram-positive bacteria (*S. aureus* and *S. pyogenes*). Obvious inhibition zone was observed in all bacteria in the presence of USCS, and the diameter of inhibition zone increased positively with the UA concentration (**Figure 4**a). Specifically, larger inhibition zone could be detected in Gram-positive bacteria, even with low UA concentration, which was relatively smaller in Gram-negative bacteria, by comparison. This result is consistent with the previous study that UA has stronger effect on Gram-positive bacteria than on Gram-negative bacteria.[25] Interestingly, with all bacteria, the inhibition zone spread evenly around the center of USCS, which might indicate that UA release was uniform and sustained.

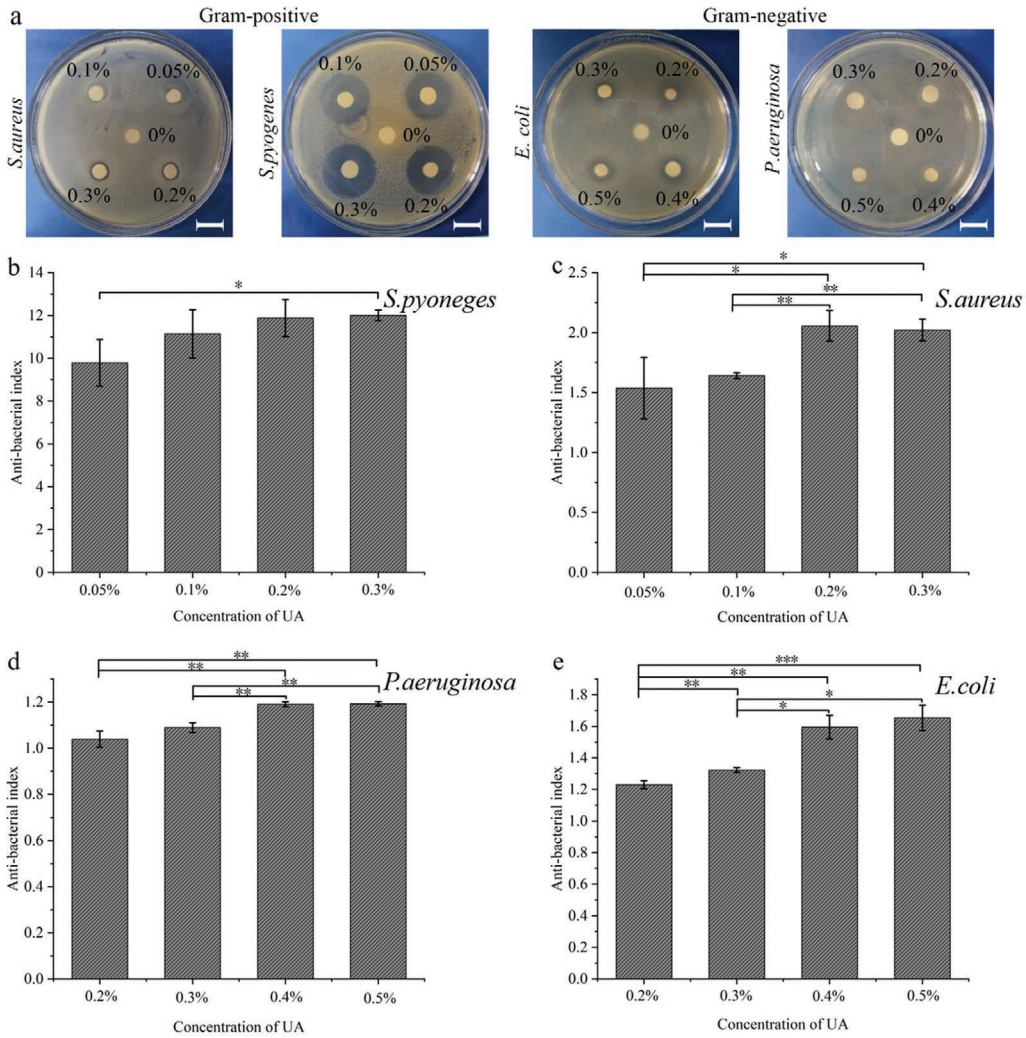

(*Continued*)

Macromolecular Bioscience
www.mbs-journal.de

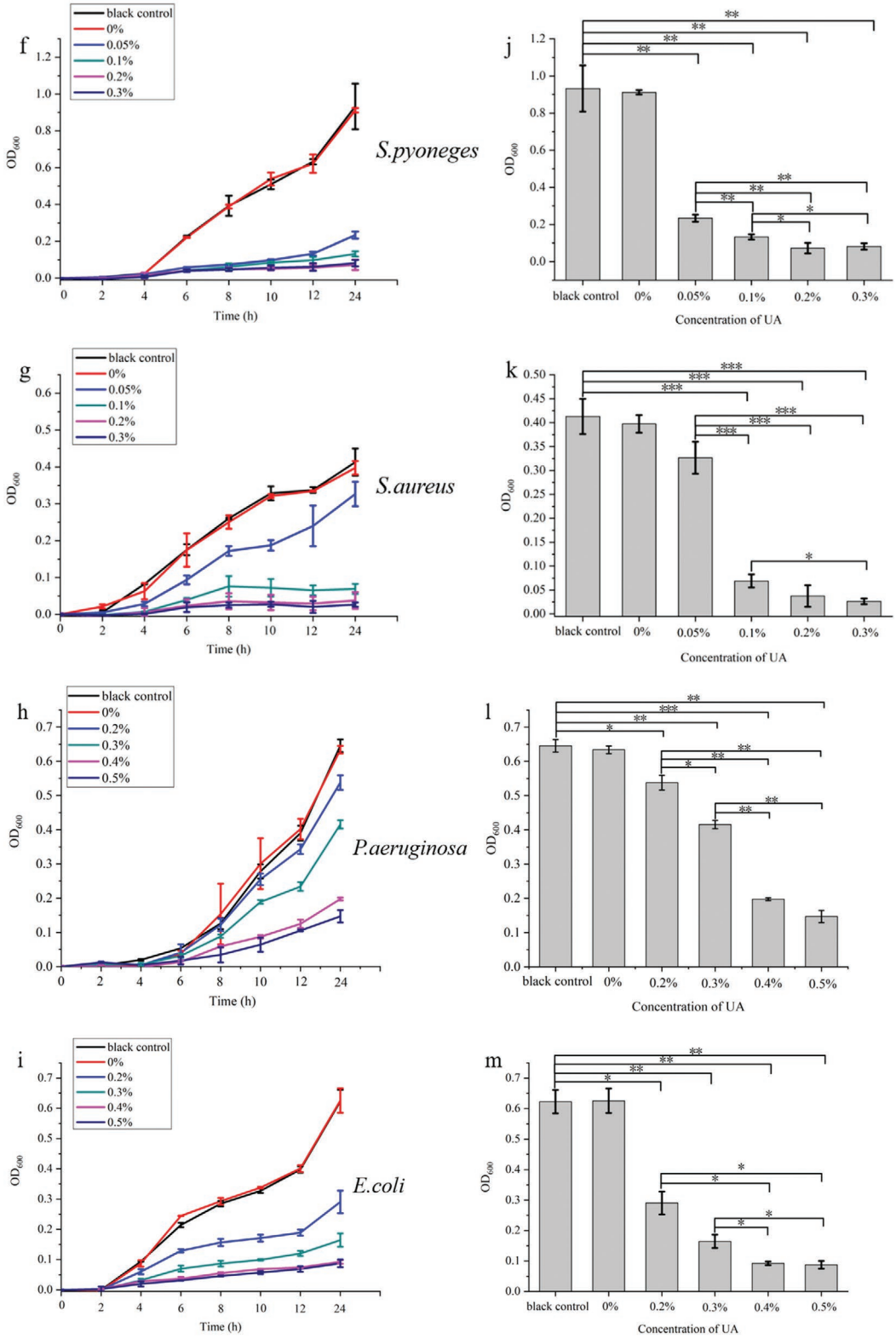

Figure 4. a) The antibacterial activity of scaffolds with and without UA. Scale bars: 10 mm. b–e) The antibacterial index of scaffolds with different concentrations of UA. f–i) The growth curves of four types bacterial. j–m) The concentration of bacterial cultured together with scaffolds at 24 h.

Furthermore, the antibacterial index was used to semiquantify the antibacterial activity of USCS. As shown in Figure 4b–e, the antibacterial index of *S. aureus* can reach about 2.02 ± 0.09, while that of *S. pyogenes* can be as high as 12.01 ± 0.25. Similarly, the inhibitory effects on *E. coli* and *P. aeruginosa* were also different, respectively, 1.65 ± 0.08 and 1.19 ± 0.01. It can be seen from the figure that inhibition degree of UA on the growth of Gram-positive bacteria was much higher than that on Gram-negative bacteria. Interestingly, 0.2% UA showed the best growth inhibition for Gram-positive bacteria and 0.4% for Gram-negative bacteria.

To further probe antibacterial activity of USCS, the growth curve of bacterial in the presence of USCS was measured in bacteria suspension assays. The bacterial growth rate was presented by optical density at 600 nm (OD_{600}) at different time points, and the final concentration at 24 h was also calculated. As shown in Figure 4f–m, the OD values of all bacterial suspensions were significantly decreased in the presence of USCS, which were consistent with inhibition zone test. For Gram-positive bacteria, significant inhibitory effect could be achieved with UA minimal concentration at 0.05% which was enhanced with the increase of UA concentration and the maximum inhibition appeared at 0.2% UA. Although, for Gram-negative bacteria, the minimum inhibitory concentration of UA was 0.2%, and the peak inhibition reached at 0.4% concentration, it is still far below the minimal concentration that UA might induce toxicity to human body,[36,37] which means USCS could be efficiently used on different bacteria types.

2.4. Biocompatibility of USCS

In the present study, USCS exhibited exceptional biocompatibility based on in vitro cell culture and cell viability test. NIH3T3 fibroblasts cultured in USCS extraction medium presented nearly identical morphology to controls (**Figure 5**a–e). This result was further confirmed by the CCK-8 cell viability test, a soluble formazan dye with the maximum absorbance at 450 nm produced as metabolically active cells react with a tetrazolium salt in the CCK-8 reagent.[38] As shown in Figure 5f, there were no significant differences in the cells viabilities among USCS with different UA concentrations and the controls, which suggested that the USCS or UA release had no significant influence on cell growth. Moreover, cells crawling fragments on USCS were observed under SEM (Figure 5g–j). Compared with controls, cells could attach to USCS with normal spreading and morphology, concluding that the prepared USCS have excellent biocompatibility.

2.5. Evaluation of Wound-Healing Performance

A cutaneous excisional mouse wound model was used to evaluate the wound-healing effect of USCS. To visualize wound closure over time, photographs of the wound region were taken on days 0, 3, 7, and 12, in which Tegaderm Hydrocolloid ^{3M}, pure SF scaffolds, and empty wound were used as positive, negative, and blank controls, respectively. As shown in **Figure 6**, USCS presented quickest wound-healing response among all groups. The wound size was significantly reduced on day 3 in the presence of USCS with a healing rate of around 53.3% ± 7.4%, while the commercial product, Tegaderm Hydrocolloid ^{3M} was only 35.4% ± 3.9%. On day 7, more significant wound closure could be observed in the USCS group compared with controls, and the healing rate reached 82.1% ± 6.4%. Moreover, open wound could be barely found in the USCS group on day 12 with the healing rate of around 96.5% ± 1.31%, which was significantly greater than positive control (81.8% ± 2.1%), negative control (78.3% ± 7.6%), and black control (57.1% ± 10.2%), respectively (Figure 6b). Previous studies have shown that SF protein alone might promote wound healing by degrading into small peptide.[1,39] However, in the present work, the pure SF scaffold did not exhibit significant difference on wound-healing effect to Tegaderm Hydrocolloid ^{3M}, which might indicate that UA sustained release from USCS should be the main cause for the promotion of wound healing.

Hematoxylin-eosin (HE) staining of tissue sections on wound site further revealed more detail information about USCS promoting wound healing. The USCS group showed slight epithelialization with more granulation tissue formation compared with controls on day 3 (**Figure 7**a,d,g,j). Besides, less infiltrated inflammatory cells could be observed in the USCS group, which might be due to the anti-inflammatory activities of UA.[25] On day 7, compared with the blank control group, little epidermis formation gradually appeared in negative and positive control groups, whereas the integrity of epidermis was much higher in USCS group at the same time. More important, ingrowth of capillaries and rejuvenation of skin appendages could be only detected in the USCS group on day 7, which indicated that healing was much faster in the USCS group. The healing stage was even more different between USCS and control groups on day 12, capillaries ingrowth and skin appendix began to appear at the wound site where was filled with immature angiogenesis in positive and negative control groups. Nevertheless, the epidermal proliferation and the epidermal layer enlargement were much more significant in the USCS group with more rejuvenation of skin appendix (Figure 7l). In addition, more assembled skin could be observed in the USCS group with compact epidermis, regenerated dermis, and standard thickness of skin layers.[40]

Skin wound healing is a multiple process, in which granulation tissue formation, collagen deposition, and angiogenesis occur simultaneously with epithelialization and wound contraction.[1] In order to elucidate the possible mechanism of USCS in promoting wound healing, Masson's Trichrome staining was conducted at first to determine the effect of USCS on collagen deposition. Theoretically, collagen deposition will begin on days 5–6 after skin injury and reach its peak on day 15.[41] As shown in **Figure 8**, the collagen deposition, represented by blue, was significantly higher in the USCS group than controls on days 3 (Figure 8a,d,g,j). Moreover, collagen deposition had reached its peak on day 7 in the USCS group, which just gradually appeared in positive and negative control groups. It could be speculated that UA sustained release from USCS could enhance expression and deposition of collagen in wound site. Besides, considering that collagen deposition is usually accompanied by angiogenesis,[30]

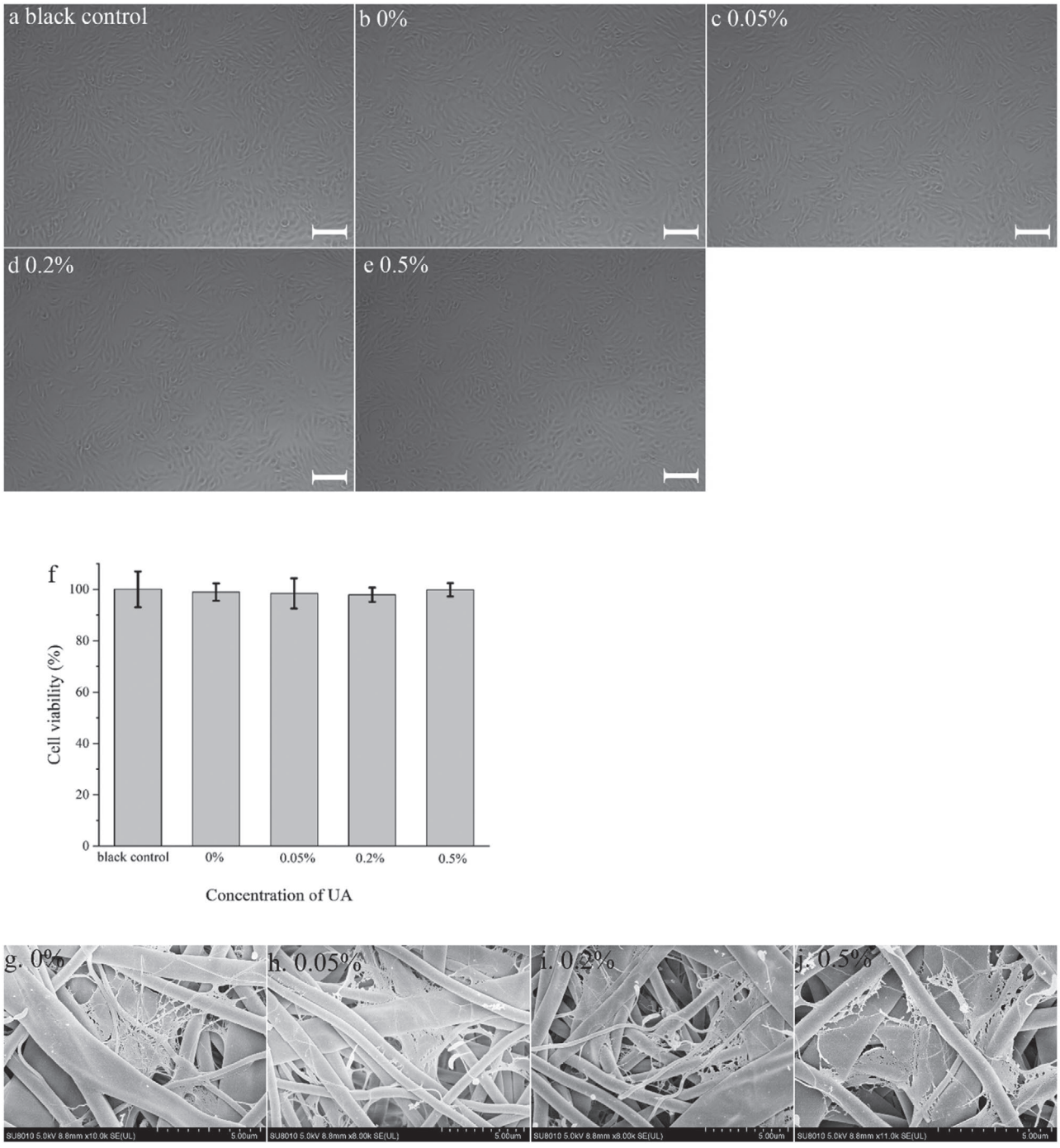

Figure 5. a–e) Cell morphology under microscope after 24 h culturing in extraction medium of USCS. Scale bars: 400 μm. f) CCK-8 cell viability test. g–j) SEM images of cells attached to USCS.

these results were consistent with HE staining which showed ingrowth of capillaries began in the USCS group on day 7. Furthermore, maturated neovascularization, hair follicles, and skin appendage were showed up in the USCS group on day 12, which indicated that the healing process was more efficient in USCS than controls (Figure 8l). These results might suggest that USCS could enhance wound healing by efficiently activating collagen deposition.

Angiogenesis is another important step of wound healing, which can provide necessary nutrition for granulation and surrounding tissues.[42,43] As mentioned before, angiogenesis was initiated promptly in the USCS group compared with controls, and the potential mechanism was also discussed in this work. Previous studies have shown that the expression of endogenous vascular endothelial growth factor (VEGF) is significantly increased during wound-healing angiogenesis, especially in the

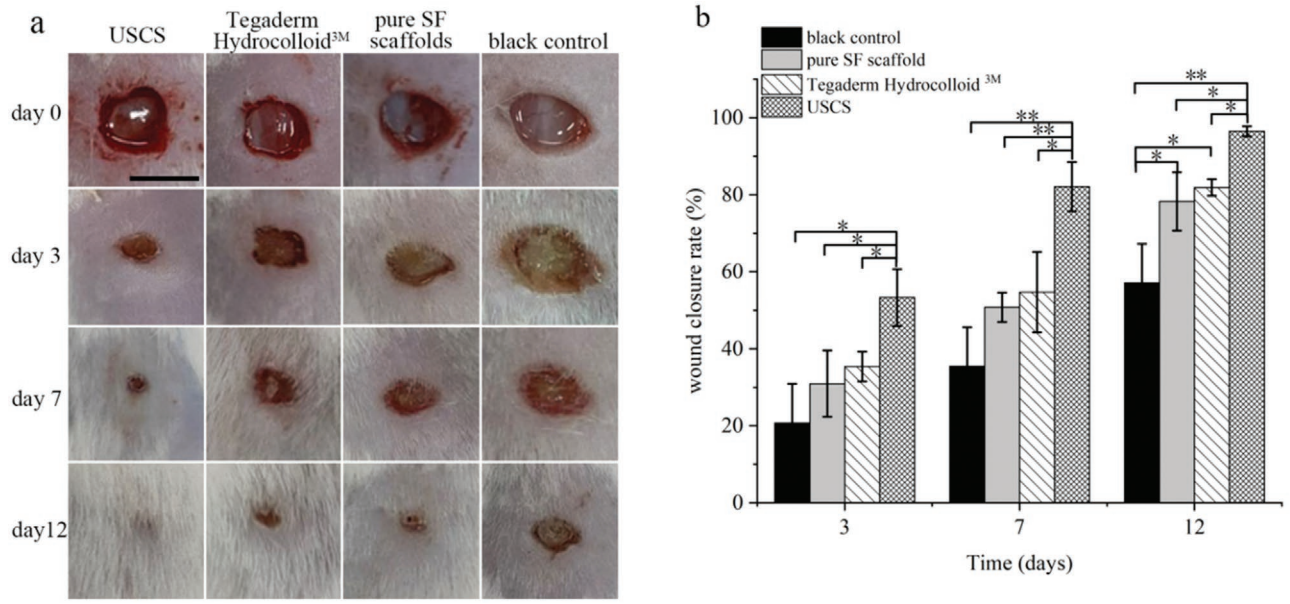

Figure 6. a) Extent of wound healing on days 0, 3, 7, and 12. b) Average wound closure rates in mice. Scale bars: 10 mm.

early stage of capillary formation;[44,45] thus, the time course of VEGF expression level was also determined by immunohistochemical analysis on days 3, 7, and 12 after wounding (**Figure 9**). The expression level of VEGF significantly increased and quickly reached its peak on day 3 in USCS group, while in control groups, it prolonged to day 7 even later to get the peak of VEGF expression. Although, the downregulation of VEGF expression showed up on day 7 in the USCS group, ingrowth of capillaries significantly began. Considering the sequence between VEGF expression and angiogenesis, it is reasonable to

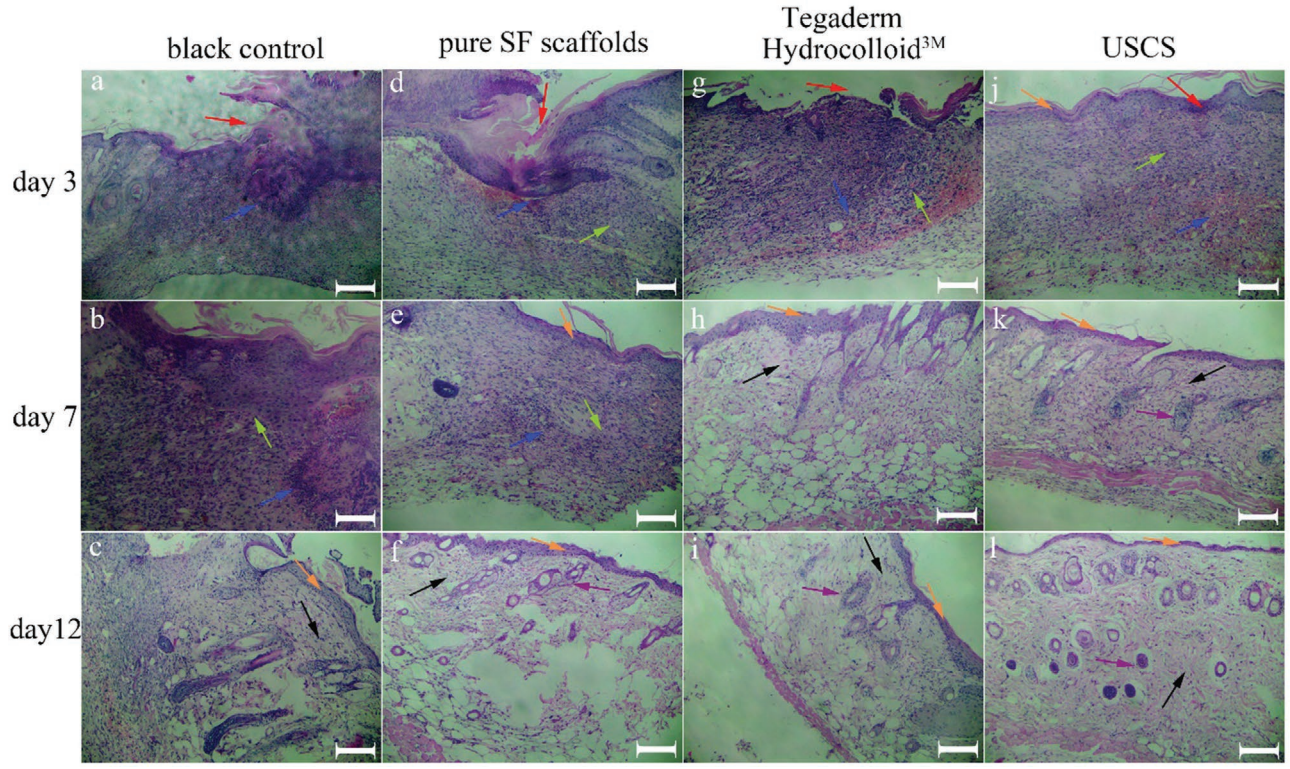

Figure 7. Hematoxylin and eosin staining images of wounds. a–c) Black control. d–f) Covered with pure SF scaffold. g–i) Covered with Tegaderm Hydrocolloid 3M. j–l) USCS treatment. Red arrows point to the punched site; orange arrows: epidermal layer; blue arrows: infiltration of inflammatory cells; purple arrows: rejuvenation of skin appendages; green arrows: new granulation tissue; black arrows: neovascularization. Scale bars: 200 μm.

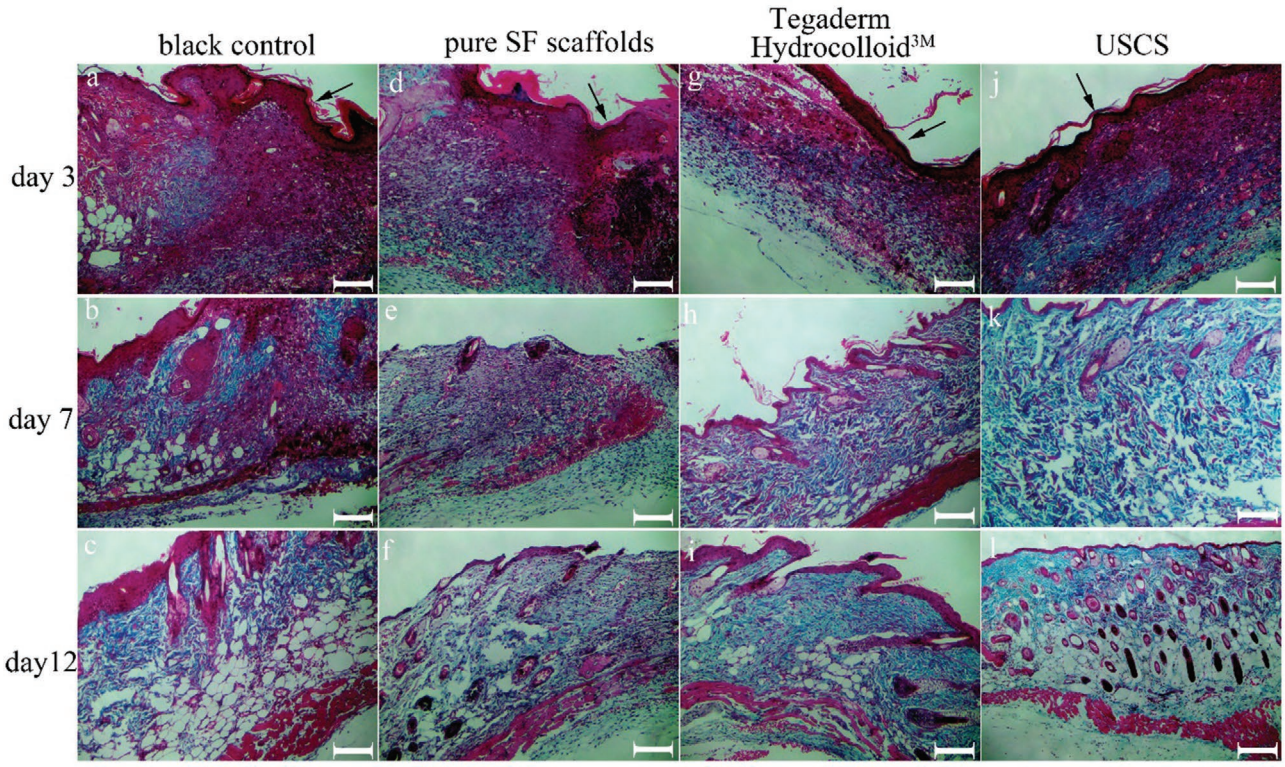

Figure 8. a) Masson's Trichrome staining images of wounds. a–c) Black control. d–f) Covered with pure SF scaffold. g–i) Covered with Tegaderm Hydrocolloid[3M]. j–l) USCS treatment. Black arrows point to the punched site; blue color represents collagen staining. Scale bars: 200 μm.

assume that USCS could advance VEGF expression to enhance wound healing.

As a major structural component of stratified epithelia, cytokeratin 10 (CK10) is a specific marker to evaluate growth of regenerated epithelial layers.[46] As shown in **Figure 10**, CK10 was first present in the wound edge covered of USCS group, while little or no expression could be detected in controls on day 3. The expression of CK10 could be observed in all groups on day 7; however, the expression level was significantly higher in the USCS group (Figure 10b,e,h,j). The highest expression of CK10 appeared on day 12 in the USCS group, where the compact epithelial layers were formed according to HE staining results. The results indicated that USCS could accelerate the formation and repair process of the epithelium to promote wound healing.

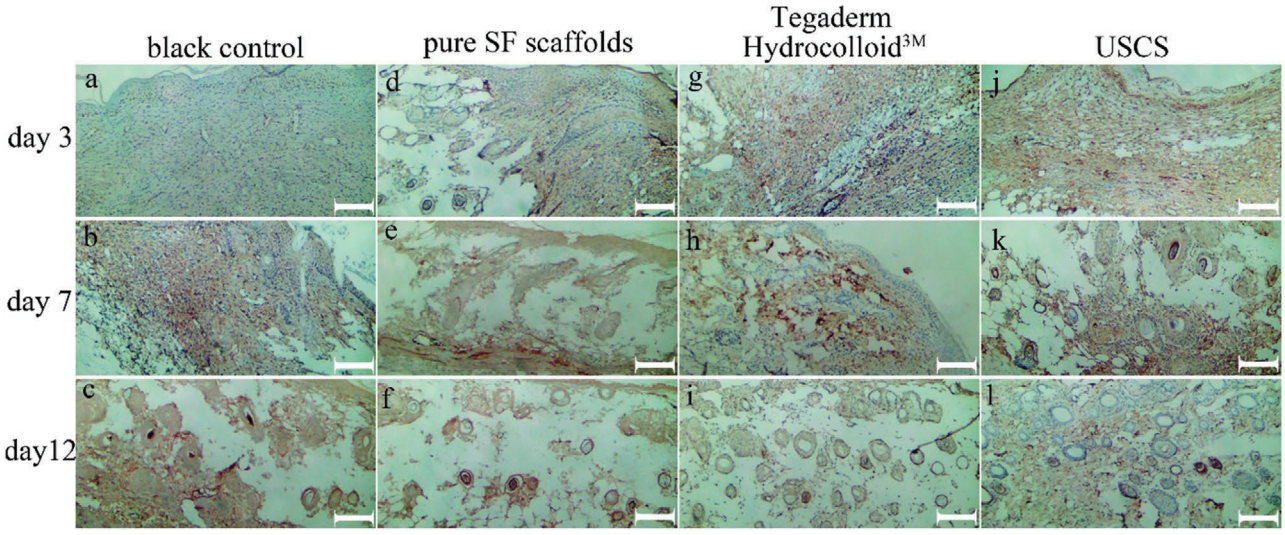

Figure 9. a) VEGF immuno-histochemistry staining images of wounds. a–c) Black control. d–f) Covered with pure silk scaffold. g–i) Covered with Tegaderm Hydrocolloid [3M]. j–l) USCS treatment. Brown part represents the intermittent VEGF expression. Scale bars: 200 μm.

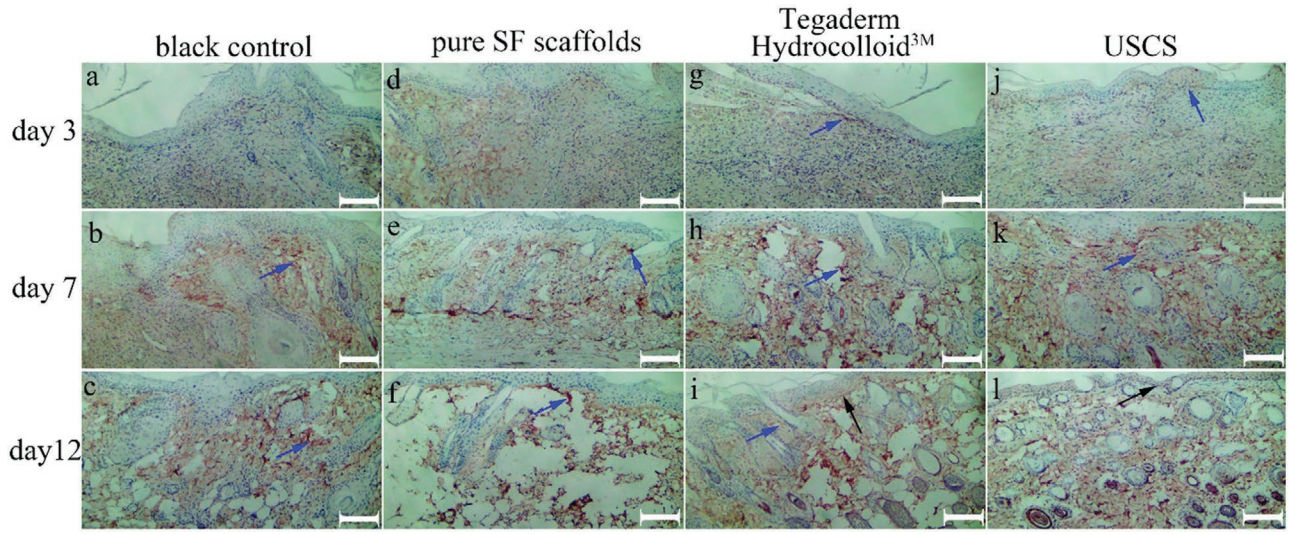

Figure 10. a) CK10 immuno-histochemistry staining images of wounds. a–c) Black control. d–f) Covered with pure silk scaffold. g–i) Covered with Tegaderm Hydrocolloid 3M. j–l) USCS treatment. Blue arrows represent the intermittent CK10 expression; black arrows point to the site of CK10 continuous expression in the integrated epidermal layer. Scale bars: 200 μm.

3. Conclusion

In the present work, we proposed a natural, biocompatible composite cutaneous scaffold, USCS with exceptional antibacterial, and wound-healing activities. Via electrospinning, SF solution mixed with UA was fabricated into a mesh structure of USCS with the average diameter of nanofibers being around 360 ± 10 nm, which granted much improved air permeability compared with commercial wound dressing, Tegaderm Hydrocolloid 3M. The mechanical properties of USCS could be tuned with different SF concentrations and methanol treatment, which promoted the flexibility (18% SF concentration:1.28% vs 20% SF concentration: 2.98%) and stiffness (in term of 20% SF concentration: before treatment (1.69 ± 0.45 Mpa) vs after treatment (2.61 ± 0.61 MPa)) respectively. With sustained release of UA, USCS exhibited significant growth inhibition on both Gram-positive and Gram-negative bacteria, including *S. aureus* (antibacterial index is 2.02 ± 0.09), *S. pyogenes* (12.01 ± 0.25), *E. coli* (1.65 ± 0.08), and *P. aeruginosa* (1.19 ± 0.01). In the model of full-thickness skin wounds on the back of mice for 12 days, USCS presented prompt wound-healing response and significantly enhance the wound closure rate (96.5% ± 1.31%) compared with the black control (57.1% ± 10.2%), pure SF scaffold (78.3% ± 7.6%), and commercial wound dressing, Tegaderm Hydrocolloid 3M (81.8% ± 2.1%). Furthermore, the potential mechanism of USCS in promoting wound healing might be summarized to enhancement of re-epithelialization, vascularization, and collagen deposition, which were benefited from USCS. Altogether, the unique combination of SF and UA might provide a new strategy for clinical treatment with chronic wound.

4. Experimental Section

Extraction of SF Aqueous Solution: Silk solution was prepared from *B. mori* cocoons according to previous studies.[4,5,15,47] Briefly, cocoons were cut into small pieces and boiled in 0.02 M sodium carbonate solution for 45 min to remove sericin protein. After rinsing, the silk material was dried and solubilized in 9.3 M lithium bromide (Shanghai Macklin Biochemical Co., Ltd.) solution at 60 °C for 4 h to obtain the initial silk solution; it was subsequently dialyzed for 2 days with dialysis bags (Beijing Solarbio Science & Technology Co., Ltd.; MWCO = 3500); and then centrifuged at 9000 rpm at 4 °C to collect SF aqueous solution (≈6 w/v%).

Preparation of USCS: SF aqueous solution was dried into films and then re-dissolved in formic acid (Shanghai Macklin Biochemical Co., Ltd.) to obtain base solutions with final SF concentrations at 18, 20, and 22 wt%.[48] Then, different mount of UA (Shanghai Macklin Biochemical Co., Ltd.) was mixed into base solution to obtain electrospinning solution with the UA final concentrations at 0.05%, 0.1%, 0.2%, 0.3%, 0.4%, and 0.5%. The electrospinning solution was placed in a 10 mL syringe capped with a needle of 0.9 mm diameter. High voltages of 15, 18, and 20 kV power supply were connected via an alligator clip to the external surface of the needle. The distance between the spinneret and the collector was 15 cm; the flow rate was 0.36–0.6 mL h^{-1}; and the process was carried out at around 23 ± 3 °C and 45% ± 5% humidity.[6,49]

Characterization of the USCS: The surface morphology of USCS was observed by SEM images (S4800, Hitachi, Chiyoda-ku, Japan) at an acceleration voltage of 5 kV with gold sputtered on the sample surfaces. USCS before and after inducing by methanol were used for FTIR analysis; the β-sheet content and contribution of the different SF conformations to the amide I region were examined by Fourier self-decomposition and curve fitting using software (OriginPro 2018; OriginLab, Corp., Northampton, USA).[5,15]

Mechanical Performance Testing: The mechanical testing of scaffolds was done according to previous method.[8] Scaffolds were cut into 20 mm × 10 mm rectangular samples, and the sample thickness was measured with a vernier caliper (Guanglu 111). The UTS was obtained when tensile tests were performed using a computer-controlled electronic universal testing machine (JJG475-2008, E43.104) equipped with a 100 N load cell at a rate of 1 mm min^{-1}, and the stress–strain data were obtained automatically.

Enzyme Degradation: USCS were cut into approximately equivalent mass (20 ± 5 mg), incubating at 37 °C in phosphate buffer solution (PBS) solution containing 3.1 U mL^{-1} protease XIV (Sigma–Aldrich, St. Louis, MO, USA).[3,4] At different time points, solutions were replaced with fresh ones; sample residues were collected, rinsed gently with ultrapure water, and dried daily, then weighed to mass remaining assessment. USCS in PBS without enzyme served as a control.

Water Vapor Transmission Rate: To detect the moisture permeability of USCS, WVTR was determined according to the standard YY/T 0471.2–2004.[34] Briefly, a circular piece of the scaffold was mounted on the top of a tube of 35.7 ± 0.1 mm diameter containing 18 mL of water, and the whole system was weighed and then incubated at 37 °C and 20% relative humidity. The WVTR (g m^{-2} day^{-1}) was calculated using the following equation[34]

$$\mathrm{WVTR} = \frac{(W_0 - W_t) \times 1000 \times 24}{T} \quad (1)$$

where W_0 and W_t are the weights of the system before and after incubation (g), respectively, and T is the length of the interval (h). Tegaderm Hydrocolloid 3M was used as a control.

UA Release: The UA release was measured according to previous studies.[15,27,50] Briefly, USCS was immersed in PBS at 37 °C and gently shaken, and the soak solution was extracted and refreshed with equal PBS at different time points. UA release was reflected by spectral changes of the extraction using a microplate reader (Multiskan, Thermo Fisher Scientific, Co., China) at 200–400 nm.

Antibacterial Test: *S. aureus*, *S. pyogenes, E. coli*, and *P. aeruginosa* were used in the antibacterial test. For the inhibition zone test, USCS was cut into pieces approximately circle, subsequently sterilized with UV radiation for 4 h. Bacteria were grown in Muller–Hinton (MH) media at 37 °C with continuous shaking for 6 h, then aliqouts (200 µL) of the bacterial suspension were manually spread on MH agar plates, followed by placing the sterile USCS on plates. After 24 h of incubation at 37 °C, the radii of inhibition zones in each plate were measured from center to edge, and the results were expressed as antibacterial index, calculated by the following equation

$$\text{Antibacterial index} = \frac{\text{Area of inhibition zone}}{\text{Area of USCS}} \quad (2)$$

For bacterial suspension assay, antibacterial activity was evaluated according to previous procedure.[38] The sterile samples and bacterial suspension were added into fresh medium, continuous shaking at 37 °C. At different time points, aliqouts of the mixture were taken out and OD_{600} was determined by a microplate reader, which was referred to as bacteria concentration.

Cytocompatibility: NIH3T3 fibroblasts were cultured in Dulbecco's modified Eagle medium (DMEM) (Gibco) supplemented with 10% fetal bovine serum (FBS) (contains penicillin/streptomycin, EVERY GREEN, Zhejiang Tianhang Biotechnology Co., Ltd.) in a humidified atmosphere of 95% and 5% CO_2 at 37 °C. Then, the culture medium was changed into USCS extraction medium and cultured in 96-well plates for 24 h; normal cultured cells were used as a control. The morphology of cells was observed under a microscope (Olympus CX23) after 24 h of incubation. Besides, CCK-8 (Solarbio, Beijing, China) assay was used to assess cell viability according to the manufacturer's instructions.[38] Briefly, CCK-8 solution was added to each well and incubated for 2 h, and then OD_{450} was measured with a microplate reader. The cell viability was defined as the ratio of OD_{450} of the treated and control groups. In addition, sterile USCS was placed in wells with 1×10^4 cells per well in 96-well plate, and then fixed with glutaraldehyde after 24 h of incubation. Cell morphology was observed by SEM at an acceleration voltage of 5 kV with sputter-coated with gold on the sample surfaces.[15,40]

In Vivo Wound Closure Rate Studies: All experiments were carried out in accordance with the guidelines of the Ethical Committee of Chongqing Medical University (CQMU). All animals were 8 weeks old male mice (Laboratory Animal Center, CQMU) and were randomly distributed by four groups each with three time points: 3, 7, and 12 days. The dorsal surfaces were shaved after anesthetization and punched 8 mm full-thickness skin wounds, treated with USCS, Tegaderm Hydrocolloid 3M, pure SF scaffold, and empty wound, were applied as experimental, positive, negative, and black control groups, respectively. Wound area was measured with ImagePro6 (Media Cybernetics, Bethesda, MD, USA) on days 0, 3, 7, and 12, and the degree of wound healing was expressed by wound closure rate, calculated by the following equation[30,34]

$$\text{wound closure rate} = \frac{A_0 - A_i}{A_0} \quad (3)$$

where A_0 and A_i are the area of original wound and the area of remaining wound after a period of treatment, respectively.

Histological Analysis and Immunostaining: Mice were sacrificed by CO_2 exposure after 3, 7, and 12 days, and the samples of full-thickness skin wound and subcutaneous tissue were collected. These samples were fixed in 4% paraformaldehyde for at least 24 h, subsequently embedded in paraffin and sectioned into a thickness of 10 µm to undergo routine histological processing with hematoxylin–eosin and Masson's Trichrome staining for histological analysis.[24,30,42,46] Primary antibodies for CK10, VEGF (Abcam, Cambridge, MA), and SP-POD kit (Solarbio Science & Technology Co., Ltd.) for immuno-histochemistry analysis.[30,42,44] Antigen retrieval was performed on sections under heating, and then incubation with a blocking reagent for 20 min. The samples were incubated at 4 °C overnight with antimouse CK10 and VEGF (diluted 1:100 in antibody diluent) after removing the blocking reagent. Subsequently, sections incubated with a secondary antibody for 30 min, incubated with SP-POD reagent for 30 min, then incubated with diaminobenzidine (DAB) coloration reagent for 20 min and washed with water to terminate the reaction. In the end, the sections were counterstained by hematoxylin, dehydrated, transparent, and sealed.

Statistical Analysis: All results were reported as mean ± standard deviation. Differences among groups were analyzed by one-way analysis of variance (ANOVA). A p-value of <0.05 was considered as a statistically significant difference.

Supporting Information

Supporting Information is available from the Wiley Online Library or from the author.

Acknowledgements

This research was supported by Chongqing Research Program of Basic Research and Frontier Technology (Program No. cstc2019jcyj-msxmX0614), Science and Technology Research Program of Chongqing Municipal Education Commission (Program No. KJQN201900414), and Smart Medicine Project of Chongqing Medical University (Grant No. ZHYX202016).

Conflict of Interest

The authors declare no conflict of interest.

Keywords

cutaneous scaffolds, electrospinning, silk fibroin, usnic acid, wound healing

Received: October 13, 2020
Revised: December 1, 2020
Published online: December 28, 2020

[1] M. Farokhi, F. Mottaghitalab, Y. Fatahi, A. Khademhosseini, D. L. Kaplan, *Trends Biotechnol.* **2018**, *36*, 907.
[2] Y.-G. Ko, M. Lee, W. H. Park, D. Cho, O. K. Kwon, O. H. Kwon, *Macromol. Res.* **2016**, *24*, 824.

[3] N. R. Raia, B. P. Partlow, M. McGill, E. P. Kimmerling, C. E. Ghezzi, D. L. Kaplan, *Biomaterials* **2017**, *131*, 58.
[4] X. Hu, K. Shmelev, L. Sun, E.-S. Gil, S.-H. Park, P. Cebe, D. L. Kaplan, *Biomacromolecules* **2011**, *12*, 1686.
[5] H. Han, H. Ning, S. Liu, Q. P. Lu, Z. Fan, H. Lu, G. Lu, D. L. Kaplan, *Adv. Funct. Mater.* **2016**, *26*, 421.
[6] Y. Kishimoto, H. Morikawa, S. Yamanaka, Y. Tamada, *Mater. Sci. Eng., C* **2017**, *73*, 498.
[7] J. Guo, C. Li, S. Ling, W. Huang, Y. Chen, D. L. Kaplan, *Biomaterials* **2017**, *145*, 44.
[8] J. Zhu, W. Huang, Q. Zhang, S. Ling, Y. Chen, D. L. Kaplan, *Materials* **2016**, *9*, 221.
[9] W. Zhang, L. S. Wray, J. Rnjak-Kovacina, L. Xu, D. Zou, S. Wang, M. Zhang, J. Dong, G. Li, D. L. Kaplan, X. Jiang, *Biomaterials* **2015**, *56*, 68.
[10] S. Zhao, Y. Chen, B. P. Partlow, A. S. Golding, P. Tseng, J. Coburn, M. B. Applegate, J. E. Moreau, F. G. Omenetto, D. L. Kaplan, *Biomaterials* **2016**, *93*, 60.
[11] W. L. Stoppel, A. E. Gao, A. M. Greaney, B. P. Partlow, R. C. Bretherton, D. L. Kaplan, L. D. Black, 3rd, *J. Biomed. Mater. Res., Part A* **2016**, *104*, 3058.
[12] W. Huang, S. Ling, C. Li, F. G. Omenetto, D. L. Kaplan, *Chem. Soc. Rev.* **2018**, *47*, 6486.
[13] H. G. Oliveira Barud, S. Barud Hda, M. Cavicchioli, T. S. do Amaral, O. B. de Oliveira Junior, D. M. Santos, A. L. Petersen, F. Celes, V. M. Borges, C. I. de Oliveira, P. F. de Oliveira, R. A. Furtado, D. C. Tavares, S. J. Ribeiro, *Carbohydr. Polym.* **2015**, *128*, 41.
[14] Y. Kishimoto, H. Morikawa, S. Yamanaka, Y. Tamada, *Mater. Sci. Eng., C* **2017**, *73*, 498.
[15] J. Song, A. Klymov, J. Shao, Y. Zhang, W. Ji, E. Kolwijck, J. A. Jansen, S. C. G. Leeuwenburgh, F. Yang, *Adv. Healthcare Mater.* **2017**, *6*, 1700014.
[16] C. Pignatelli, G. Perotto, M. Nardini, R. Cancedda, M. Mastrogiacomo, A. Athanassiou, *Acta Biomater.* **2018**, *73*, 365.
[17] Q. Niu, Q. Peng, L. Lu, S. Fan, H. Shao, H. Zhang, R. Wu, B. S. Hsiao, Y. Zhang, *ACS Nano* **2018**, *12*, 11860.
[18] S. Li, L. Li, C. Guo, H. Qin, X. Yu, *Int. J. Biol. Macromol.* **2017**, *104*, 969.
[19] L. Zhou, Q. Wang, J. Wen, X. Chen, Z. Shao, *Polymer* **2013**, *54*, 5035.
[20] X. Li, Y. Liu, J. Zhang, R. You, J. Qu, M. Li, *Mater. Sci. Eng., C* **2017**, *72*, 394.
[21] H. Gong, J. Wang, J. Zhang, J. Wu, Z. Zheng, X. Xie, D. L. Kaplan, G. Li, X. Wang, *Mater. Sci. Eng., C* **2019**, *102*, 820.
[22] A. Sugihara, K. Sugiura, H. Morita, T. Ninagawa, K. Tubouchi, R. Tobe, M. Lzumiya, T. Horio, N. G. Abraham, S. Lkehara, *Proc. Soc. Exp. Biol. Med.* **2000**, *225*, 58.
[23] P. J. Babu, M. Doble, A. M. Raichur, *J. Colloid Interface Sci.* **2018**, *513*, 62.
[24] G. Gowda, A. H. Shivalingaiah, A. M. Vijayeendra, N. Sarkar, C. Nagaraj, N. R. Masthi, *Asia Pac. Allergy* **2016**, *6*, 90.
[25] I. Francolini, A. Piozzi, G. Donelli, *Adv. Exp. Med. Biol.* **2019**, *1214*, 31.
[26] Y. N. Antonenko, L. S. Khailova, T. I. Rokitskaya, E. S. Nosikova, P. A. Nazarov, O. A. Luzina, N. F. Salakhutdinov, E. A. Kotova, *Biochim. Biophys. Acta, Bioenerg.* **2019**, *1860*, 310.
[27] A. Martinelli, A. Bakry, L. D'Ilario, I. Francolini, A. Piozzi, V. Taresco, *Eur. J. Pharm. Biopharm.* **2014**, *88*, 415.
[28] M. R. Dos Santos, J. J. Alcaraz-Espinoza, M. M. da Costa, H. P. de Oliveira, *Mater. Sci. Eng., C* **2018**, *89*, 33.
[29] P. Nithyanand, R. M. Beema Shafreen, S. Muthamil, S. Karutha Pandian, *Microbiol. Res.* **2015**, *179*, 20.
[30] Z. Zhang, Y. Zheng, Y. Li, H. Bai, T. Ma, X. Song, J. Zhao, L. Gao, *Biomed. Pharmacother.* **2018**, *97*, 587.
[31] E. S. Araújo, E. C. Pereira, M. M. da Costa, N. H. da Silva, H. P. de Oliveira, *Nanotechnology* **2016**, *10*, 252.
[32] C. Pagano, M. R. Ceccarini, P. Calarco, S. Scuota, C. Conte, S. Primavilla, M. Ricci, L. Perioli, *Colloids Surf., B* **2019**, *178*, 488.
[33] M. A. de Moraes, C. R. Albrecht Mahl, M. Ferreira Silva, M. M. Beppu, *J. Appl. Polym. Sci.* **2015**, *132*, 41802.
[34] F. Zhou, W. Wang, H. Guo, *J. Biomater. Appl.* **2019**, *33*, 1434.
[35] B. Sahu, A. Prusty, B. Tudu, *J. Orthop. Surg.* **2018**, *26*, 230949901880248.
[36] L. F. Leandro, C. C. Munari, V. L. Sato, J. M. Alves, P. F. de Oliveira, D. F. Mastrocola, P. Martins Sde, S. Moraes Tda, A. I. de Oliveira, M. G. Tozatti, W. R. Cunha, D. C. Tavares, *Mutat. Res.* **2013**, *753*, 101.
[37] I. Prokopiev, G. Filippova, E. Filippov, I. Voronov, I. Sleptsov, A. Zhanataev, *Mutat. Res., Genet. Toxicol. Environ. Mutagen.* **2019**, *839*, 36.
[38] M. Yang, Y. Wang, G. Tao, R. Cai, P. Wang, L. Liu, L. Ai, H. Zuo, P. Zhao, A. Umar, C. Mao, H. He, *Nanomaterials* **2018**, *8*, 235.
[39] A. E. Thurber, F. G. Omenetto, D. L. Kaplan, *Biomaterials* **2015**, *71*, 145.
[40] H. Samadian, S. Zamiri, A. Ehterami, S. Farzamfar, A. Vaez, H. Khastar, M. Alam, A. Ai, H. Derakhshankhah, Z. Allahyari, A. Goodarzi, M. Salehi, *Sci. Rep.* **2020**, *10*, 8312.
[41] G. Han, R. Ceilley, *Adv. Ther.* **2017**, *34*, 599.
[42] W. Y. Zhao, Q. Q. Fang, X. F. Wang, X. W. Wang, T. Zhang, B. H. Shi, B. Zheng, D. D. Zhang, Y. Y. Hu, L. Ma, W. Q. Tan, *Wound Repair Regen.* **2020**, *28*, 326.
[43] M. Takeo, W. Lee, M. Ito, *Cold Spring Harbor Perspect. Med.* **2015**, *5*, a023267.
[44] D. W. Sant, V. Camarena, S. Mustafi, Y. Li, Z. Wilkes, D. Van Booven, R. Wen, G. Wang, *Invest. Ophthalmol. Visual Sci.* **2018**, *59*, 3608.
[45] R. S. Apte, D. S. Chen, N. Ferrara, *Cell* **2019**, *176*, 1248.
[46] E. S. Gil, B. Panilaitis, E. Bellas, D. L. Kaplan, *Adv. Healthcare Mater.* **2013**, *2*, 206.
[47] Z. Zhou, Z. Shi, X. Cai, S. Zhang, S. G. Corder, X. Li, Y. Zhang, G. Zhang, L. Chen, M. Liu, D. L. Kaplan, F. G. Omenetto, Y. Mao, Z. Tao, T. H. Tao, *Adv. Mater.* **2017**, *29*, 1605471.
[48] L. Pang, J. Ming, F. Pan, X. Ning, *Polymers* **2019**, *11*.
[49] H. Cao, X. Chen, L. Huang, Z. Shao, *Mater. Sci. Eng., C* **2009**, *29*, 2270.
[50] E. M. Pritchard, T. Valentin, B. Panilaitis, F. Omenetto, D. L. Kaplan, *Adv. Funct. Mater.* **2013**, *23*, 854.